ELSEVIER

Journal of Nuclear Materials 300 (2002) 151–160

journal of nuclear materials

www.elsevier.com/locate/jnucmat

Order–disorder phase transition induced by swift ions in $MgAl_2O_4$ and $ZnAl_2O_4$ spinels

D. Simeone [a,*], C. Dodane-Thiriet [b], D. Gosset [a], P. Daniel [c], M. Beauvy [b]

[a] *Laboratoire de Métallurgie et d'Etude de l'Endommagement, DEN/DMN/SEMI/LM2E, CEA, CEA Saclay, F-91191 Gif-sur-Yvette cedex, France*

[b] *Laboratoire des Lois du Comportement du Combustible, DEN/DEC/SESC, CEA, CEA Cadarache, F-13108 St Paul Lez Durance, France*

[c] *Laboratoire de Physique de l'Etat Condensé, UPRES A CNRS 6087, F-72085, Le Mans cedex, France*

Received 16 August 2001; accepted 12 November 2001

Abstract

Grazing X-ray diffraction was used to study in details the behaviour of two spinels, $ZnAl_2O_4$ and $MgAl_2O_4$ irradiated by swift ions. Such an irradiation allows to have an important irradiated depth and then accurate diffraction diagrams. Rietveld refinement done on these diagrams clearly show an order–disorder transition due to a melting of cations under irradiation in these two spinels. More especially, these results clearly exhibit that no new phase is created under irradiation in $MgAl_2O_4$. Raman spectroscopy, sensitive to the crystallographic space group, seems to confirm this analysis.

1. Introduction

A possible way to decrease the quantity of minor actinides such as neptunium, americium and curium produced in nuclear plants, is to break down these heavy nuclei under neutron bombardment. To transmute these nuclei, one needs to insert these elements in a matrix that stays stable under neutron irradiation. $MgAl_2O_4$ is a potential material for matrix. Many studies clearly show that such matrices are resistant under neutron irradiation [1].

The crystal spinel structure (noted AB_2O_4) consists of a cubic cell that belongs to the space group $Fd\bar{3}m$. This cubic cell contains a close packed array of 32 oxygen atoms with cations in tetrahedral and octahedral interstices. In the normal spinel structure, 8 tetrahedral sites (out of 64 in a unit cell) are occupied by divalent cations, whereas 16 octahedral sites (out of 32 in a unit cell) are occupied by trivalent cations. $MgAl_2O_4$ is the more common of the spinel structural family. Their natural minerals and $ZnAl_2O_4$ minerals too have the normal structure in which Mg^{2+} (or Zn^{2+}) ions are located at tetrahedral sites (8a in Wyckoff notation, point symmetry $\bar{4}3m$), Al^{3+} ions at octahedral sites (16d in Wyckoff notation point symmetry $\bar{3}m$) and O^{2-} ions at positions (u,u,u) (32e in Wyckoff notation point symmetry 3m) [2]. However, in synthetics spinels, a disordered distribution of cations among these polyhedra exists systematically. This cation disorder is quantified in terms of an inversion parameter that specifies the fraction of trivalent aluminium ions that occupy tetrahedral sites.

Among this family, $MgAl_2O_4$ has been extensively analysed. Many authors studied its structural modifications under neutron irradiation [1], low energetic ions [3] and heavy energetic ions [4]. Although some dislocation loops appear during neutron irradiation in single crystals, there is no clear evidence of the apparition of extended defects such as dislocation networks likely to induce an important swelling [5]. This matrix does not

* Corresponding author. Tel.: +33-1 69 08 29 20; fax: +33-1 69 08 90 82.

E-mail address: david.simeone@cea.fr (D. Simeone).

0022-3115/02/$ - see front matter
PII: S0022-3115(01)00749-8

seem to be affected by radiation damage until important displacement per atoms (dpa) values.

Under 400 keV Xe irradiation at cryogenic temperatures, some authors observed an amorphisation of $MgAl_2O_4$ at an high fluence [6]. Based on an analysis of intensity spots of TEM diffraction patterns, some authors claim that $MgAl_2O_4$ reaches a new metastable state under ion irradiation [7,8] before amorphisation. However, these results disagree with previous Rietveld refinements on neutron diffraction diagrams made on $MgAl_2O_4$ single crystal irradiated under high neutron fluxes [9].

Until now, no clear theoretical works [10,11] have neither been able to explain nor to predict the behaviour of insulators under irradiation. Some attempts were done to quantify colour centres (point defects) created by irradiation. However, no clear links exist between these defects and a macroscopic functional, analogous to the partition function at equilibrium, describing the evolution, for instance amorphisation, of these materials under irradiation. The first step to discuss the existence of such a functional far from equilibrium is to obtain clear and available information on the behaviour of various insulators under irradiation. Among these, ZrO_2 has been extensively studied. This material undergoes under irradiation a displacive phase transformation that could be described in the same theoretical framework as the behaviour of spinels.

To obtain accurate information on the behaviour of spinels under irradiation (modification of the space group during irradiation), $MgAl_2O_4$ and $ZnAl_2O_4$, were irradiated by swift Kr ions at room temperature and analysed using X-ray diffraction technique.

Since the X-ray atomic form factors associated to Mg and Al atoms are similar, extinction of diffraction lines may occur; which would lead to a false determination of the space group of $MgAl_2O_4$ obtained by the analysis of X-ray diffraction diagrams. Moreover, a mixing coefficient of the two species Mg and Al would be hardly obtained. In $ZnAl_2O_4$, Zn and Al atoms have different atomic form factors and these drawbacks cannot occur.

To validate the crystallographic structure obtained by the Rietveld analysis of the X-ray diffraction diagrams on $MgAl_2O_4$ and $ZnAl_2O_4$, the Raman spectroscopy was used. All these results lead us to propose a mechanism to explain the transformation of the spinels under irradiation.

2. Experimental procedure

2.1. Sample preparation

2.1.1. $ZnAl_2O_4$ preparation

A ZnO powder with a purity of 99.99% and a Al_2O_3 powder with a purity of 99%, were blended and calcinated 1 h at 1473 K to obtain an $ZnAl_2O_4$ powder. This compacted powder was sintered 8 h at 1673 K under atmospheric pressure. These pellets were cut to obtain discs (with a diameter of 12 mm and a thickness of 1 mm) with a density equal to 67% of the theoretical density (4.58 $g\,cm^{-3}$). The grain size measured by scanning electronic microscopy (SEM) was about 0.4 μm. The grain distribution was isotropic. Samples were polished (specular) to collect accurate X-ray diffraction diagrams.

2.1.2. $MgAl_2O_4$ preparation

$MgAl_2O_4$ powder produced by the Baikowsky company contains 4 ppm (a.w.) of Na, 77 ppm of K (a.w.), 11 ppm (a.w.) of Fe, 10 ppm (a.w.) of Si and 2 ppm (a.w.) of Ca impurities. Moreover, 1.2% (a.w.) of MgO and 0.3% (a.w.) of Al_2O_3 remain free in this powder. A sample of this powder was sintered one hour at 1923 K under H_2 with H_2O (2% vol.) atmosphere after pressing (300 MPa). This sintering process permits to obtain high density pellets (98% of the theoretical density, i.e. 3.51 $g\,cm^{-3}$). These pellets were cut to obtain discs (with a diameter of 8 mm and a thickness of 2 mm). The grain size measured by SEM was about 3 μm. The grain distribution was isotropic. Samples were polished (specular) to collect accurate X-ray diffraction diagrams.

2.2. X-ray diffraction

To study the crystallographic evolution of $MgAl_2O_4$ and $ZnAl_2O_4$ samples irradiated by Kr ions, X-ray diffraction was used. An INEL diffraction set-up was used to perform the small incidence X-ray experiments with the main following characteristics [12]:

- fine (3 mm × 30 μm) parallel monochromatic X-ray beam (CuKα1 selected with a flat Ge(1 1 1) monochromator),
- accurate positioning of the sample on a rotating holder mounted on a goniometer head (residual precession $< \pm 0.02°$, height ± 1 μm, incidence angle $\pm 0.02°$),
- angular calibration of the curved position sensitive detector (8192 channels for 120°, i.e. 0.015°/channel) with a Y_2O_3 standard (cubic, $a = 10.015$ Å, i.e. 62 diffraction lines in the range 20–120° 2θ),
- yield correction for the recorded spectrum with a ZnS fluorescent sample.

Fig. 1 presents the evolution of the X-ray penetration depth, in which 90% of X-ray are diffracted, as a function of the incident angle in $MgAl_2O_4$ and $ZnAl_2O_4$.

2.3. Raman spectrometry

The Raman spectra of irradiated samples were recorded in a back-scattering configuration, under mi-

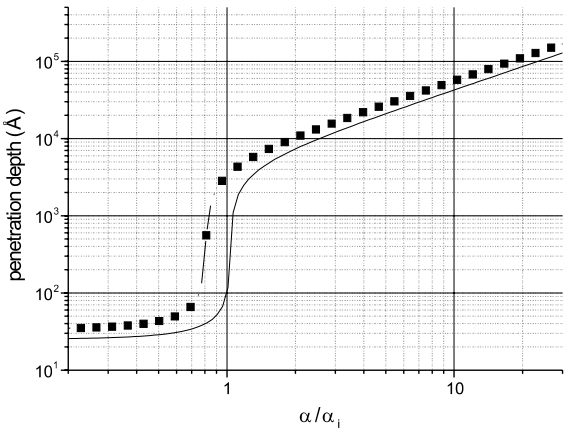

Fig. 1. Evolution of the penetration depth of X-rays for $MgAl_2O_4$ (—) and $ZnAl_2O_4$ (■) as a function of the incidence angle in grazing X-ray diffraction. This calculation was done for CuKα1 radiation. The density and critical angle of $MgAl_2O_4$ and $ZnAl_2O_4$ spinels were respectively 3.51 g cm^{-3}, 3.07 g cm^{-3}, 0.27° and 0.25°.

croscope, by using a T64000 Jobin-Yvon ISA multichannel Raman spectrometer with a CCD detector. A confocal hole coupled with the microscope was adjusted to its minimum value in order to enhance the signal coming from the irradiated surface. The 514.5 and 488 nm excitation laser lines used (coherent argon-krypton ion laser) were tested together on the samples, in order to avoid the luminescence signal due to impurities. A laser beam power that does not exceed an approximate level of 20 mW was chosen. It was checked that the laser beam light did not damage the surface of the samples.

2.4. Samples irradiations

Two kinds of irradiation were performed on $MgAl_2O_4$ and $ZnAl_2O_4$ polycrystalline samples at the GANIL facility. The interest of using high energetic ions to irradiate spinels can be summarised in two distinct points:

(1) Having a large, uniformly irradiated volume (with a thickness of about 20 μm: see Fig. 2). The good quality of the collected X-ray diffraction diagrams on these samples allow us to use the Rietveld method to determine accurately the phase modifications induced by irradiation.

(2) Probing only the volume damaged in the constant electronic stopping power range (11 and 14 keV nm^{-1} for $MgAl_2O_4$ and 9 keV nm^{-1} for $ZnAl_2O_4$). It will then be possible to analyse the new phase only due to inelastic collisions, and to compare it with the phase produced by displacement cascades [8,9].

For these reasons, different $MgAl_2O_4$ spinels were irradiated by Kr^{32+} ions with a kinetic energy of 765 and 412 MeV to a fluence of 10^{14} ions cm^{-2}, and $ZnAl_2O_4$ spinels were irradiated by Kr^{32+} ions with a kinetic energy of 765 MeV to a fluence of 10^{14} ions cm^{-2}. The program SRIM2000 was used to calculate the inelastic energy loss and dpa profiles in the two spinels as a function of the penetration depth of Kr ions in the matrix (cf. Fig. 2(a) and (b)). For these calculations, the threshold energies were fixed at 30 eV for Mg, Zn and Al atoms and 60 eV for oxygen atoms [1]. The interest of such a calculation is only to clearly define area where the inelastic energy loss predominates. The exact values of the displacement thresholds for different atoms do not play any part in this determination.

3. Experimental results

Grazing X-ray diffraction diagrams were analysed by the Rietveld method. The quality of the collected diffraction diagrams allow us to use the Rietveld method to analyse modifications induced in ceramics by

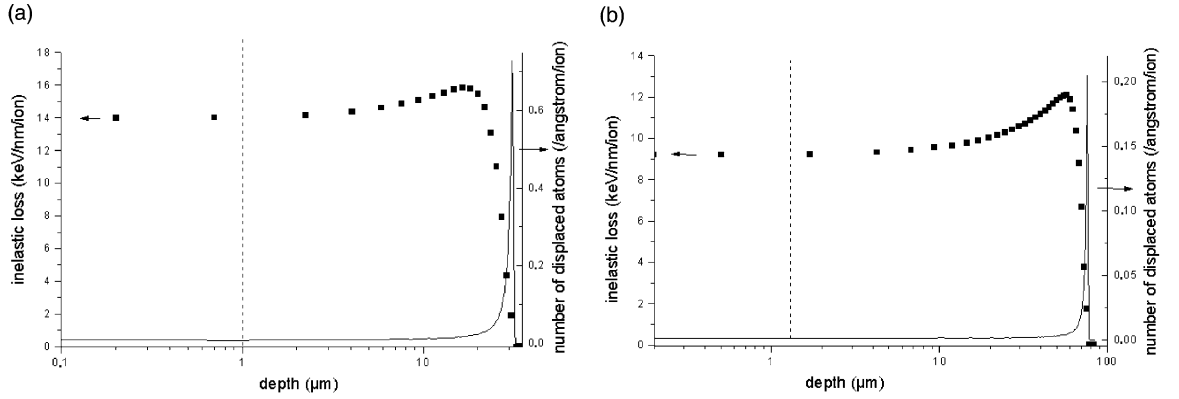

Fig. 2. Profiles of inelastic energy losses (■) and dpa (—) as a function of the penetration depth of Kr ions in $MgAl_2O_4$ (a) and $ZnAl_2O_4$ (b) samples described in the text. The vertical dash lines define the maximum penetration depth of X-ray for $MgAl_2O_4$ (1.02 μm) and $ZnAl_2O_4$ (1.15 μm), i.e., the probed volume.

irradiation, which permits one to compute accurately the different positions of atoms and their sites occupancies. Moreover, information on the global and local strain fields can be obtained by analysing respectively the position and broadening of Bragg peaks [13].

3.1. X-ray diffraction

A Rietveld program (XND software [14]) modified to take into account specific errors on Bragg peaks broadening associated to grazing incidence [12], was used to extract these information from CuKα1 X-ray diffraction diagrams. Table 1 presents the estimators associated to different Rietveld analyses and the number of parameters used in the simulations. Because CuKα1 radiation was the only radiation used in this study, only isotropic global Debye–Waller factors were used in the Rietveld refinement. The penetration depths of area probed by X-rays were equal to 1.1 μm for $ZnAl_2O_4$ (0.8° for the incident X-ray beam) and 1 μm (0.7°) for $MgAl_2O_4$.

Rietveld refinement was carried both on irradiated and unirradiated samples on X-ray diffraction diagrams collected under an incident angle of 0.8°. Figs. 3 and 4 present the results of the Rietveld refinements made on unirradiated and irradiated samples. The GofF values of the Rietveld refinement are quite important (Table 1). One fact explains the high value of this estimator. The X-ray diffraction is over collected (i.e. collected over a long time), leading to a low R_{exp}. The R_{Bragg} is quite good. The accuracy on the atomic positions of all the atoms, especially the u parameter, is also good because all species in these spinels have similar atomic form factor which do not differ more than a factor 2.

3.1.1. Rietveld analysis on unirradiated and irradiated $ZnAl_2O_4$

The form of the Bragg peaks does not reveal any strain field in the unirradiated and irradiated materials. Moreover, the coherent diffracting domains (CDD) remain roughly equal before and after the irradiation.

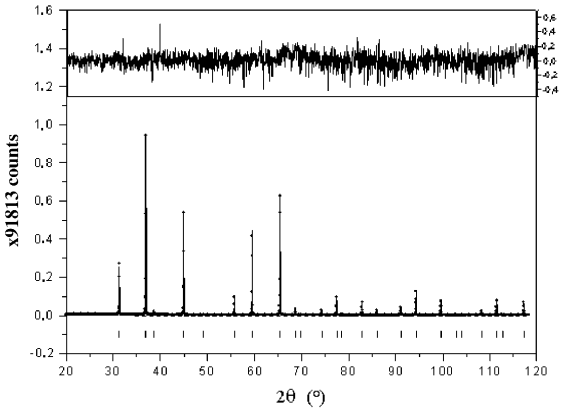

Fig. 3. Rietveld refinement on an unirradiated $ZnAl_2O_4$ sample, black lozenges: experimental X-ray diffraction diagram, black curve: simulated X-ray diagram, black triangles: simulated background, bars: Bragg angles associated to the phase, black curve on the top of the graph: fractional difference $(y_{exp} - y_{cal})/y_{exp}$ in each point divided by the standard deviation.

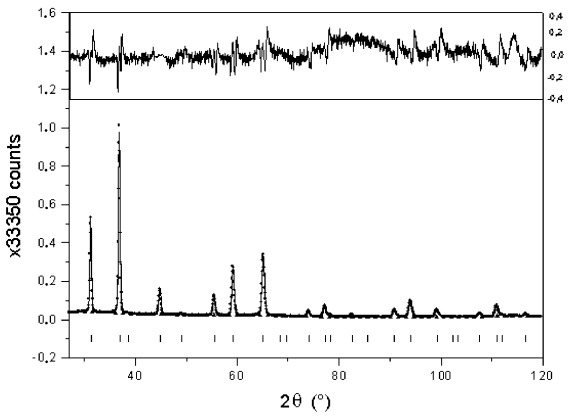

Fig. 4. Rietveld refinement on an irradiated $ZnAl_2O_4$ sample.

Table 1
Estimators used to define the quality of Rietveld refinements and the phases and Wickoff positions of cations and anions used to simulate the experimental X-ray diffraction diagrams

	R_{wp}	R_B	GofF	d_{DW}	Crystallographic phase used for the refinement	Number of parameters
$MgAl_2O_4$ unirradiated	9.44	3.06	1.67	1.32	$Fd\bar{3}m$	14
$MgAl_2O_4$ irradiated	4.66 collected 6 days	4.27	3.46	1.85	$Fm\bar{3}m$	13
$ZnAl_2O_4$ unirradiated	8.94	4.28	2.94	1.86	$Fd\bar{3}m$	11
$ZnAl_2O_4$ irradiated	6.17	3.28	2.17	1.77	$Fd\bar{3}m$	12

The GofF values are important because diffraction X-ray diagrams are always over-collected. Moreover, the important value of GofF for irradiated $ZnAl_2O_4$ spinel is due to a rough simulation of Bragg peaks broadening, as shown by the Hall Williamson plots. The Bragg estimator characterising the expected space group in the Rietveld refinement agrees quite well for all samples. The Durbin Watson estimator (d_{DW}) describing correlation between Bragg peaks is correct.

Table 2
Evolution of the unit cell parameter (a), atomic position of oxygen anion (u), isotropic Debye–Waller factors (B_{iso}), occupation of different tetrahedral and octahedral sites, and sizes of CDD (β) and slopes (η) of the Hall Williamson plot

	a (nm)	u (origin in $\bar{3}$m)	B_{iso} (nm^2)	Occupations	β (μm)	η
$MgAl_2O_4$ unirradiated	0.80676(4)	0.26159(9)	0.0080(3)	$Mg_T = 0.756(6)$ $Al_T = 0.242(6)$ $Mg_O = 0.123(2)$ $Al_O = 1.839(2)$	0.5	0
$MgAl_2O_4$ irradiated	0.40304(6)	0.5(fixed)	$B_O = 0.018(6)$ $B_{SP} = 0.013(6)$	$O = 0.983(4)$ $SP_T = 0.158(2)$ $SP_O = 0.619(2)$	0.8	0.012
$ZnAl_2O_4$ unirradiated	0.80847(8)	0.2634(1)	0.0155(2)	$Zn_T = 0.920(1)$ $Al_T = 0.078(1)$ $Zn_O = 0.078(1)$ $Al_O = 1.920(1)$	0.06	0
$ZnAl_2O_4$ irradiated	0.80952(3)	0.2605(1)	0.0132(2)	$Zn_T = 0.585(1)$ $Al_T = 0.408(1)$ $Zn_O = 0.408(1)$ $Al_O = 1.585(3)$	0.12	0

SP abbreviation is for the Al–Mg fictitious atom defined in the text. For $ZnAl_2O_4$, β are similar showing no clear evolution of CDD with irradiation. For the irradiated $MgAl_2O_4$ spinel, a clear strain field (non-null η value) appears during irradiation without any change of CDD.

Table 2 presents the evolution of the parameter u and the sites occupation of Zn and Al cations in octahedral and tetrahedral positions. The inversion parameter obtained by the Rietveld analysis on unirradiated samples is equal to 0.078. An NMR study on the same powders before irradiation exhibits an inversion parameter of 0.084 and then confirms the value obtained by the Rietveld refinement. Moreover, the lattice parameter (0.80847 nm) and the oxygen atomic position agree with previous empirical works linking the lattice parameter with the inversion parameter in these spinels [2]. The oxygen parameter u agrees with previous results [2] on annealed $ZnAl_2O_4$ spinels.

The X-ray diffraction diagrams of unirradiated and irradiated samples differ only on the intensities and positions of Bragg peaks. This variation of intensity does not decrease as a function of the diffraction angle and then cannot be explained only by an increasing of Debye–Waller factors. The only way to explain such variations of intensity is to modify the occupation sites of Zn and Al on cations sites. Rietveld refinements with variable occupation sites on tetrahedron and octahedron were carried on and results are presented in Table 2. These refinements exhibit an important increase of the inversion parameter (0.40) in probed irradiated area.

From these refinements, it is clear that an order–disorder transition occurs (drastic modifications of the inversion parameter) during irradiation. The driving force of this transition is induced by the energy deposited by electronic collisions without any further change of the crystallography of this material.

3.1.2. Rietveld analysis on unirradiated and irradiated $MgAl_2O_4$

A Rietveld refinement was done on the unirradiated $MgAl_2O_4$ sample. Tables 1 and 2 present the results and estimators of this refinement. Both GofF and R_{Bragg} are acceptable values. The comparison between experimental and calculated X-ray diagrams is plotted on Fig. 5.

The analysis of the integral broadening exhibits no strain field and large CDD (in agreement with the grain size). The analysis of the sites occupancy shows that the elaborated spinel is not stoichiometric ($Mg/Al < 0.5$). Therefore no comparison of the lattice parameter a

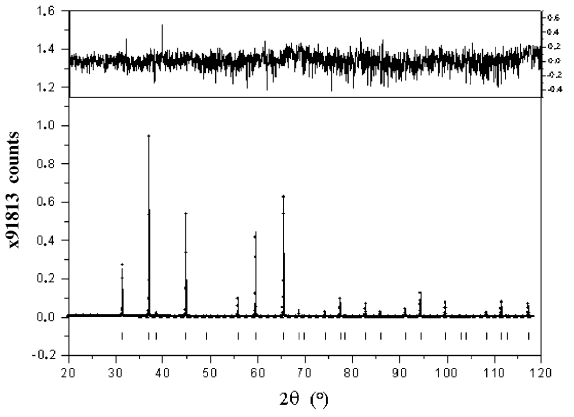

Fig. 5. Rietveld refinement on an unirradiated $MgAl_2O_4$ sample.

(0.80677(3) nm), the inversion parameter and the oxygen reduced position u can be done because no data exist on non-stoichiometric $MgAl_2O_4$ spinels [15].

After irradiation, X-ray diffraction diagrams appear very different from the unirradiated ones which define the spinel. On the samples irradiated by 765 and 412 MeV Kr ions, bumps (near 35° and 62°) clearly appear (Fig. 6). These are associated to an significant amorphisation of the spinel, in agreement with previous results [4]. Because of this increase of the background, only samples irradiated by 412 MeV Kr ions were analysed by the Rietveld method. However, X-ray diffraction diagrams of samples irradiated at the two energies exhibit similar features and Bragg peaks. In addition, irradiation induces the disappearance of the peak at 38° in both samples.

Irradiation by 400 keV Xe ions at cryogenic temperature [7], neutrons [9], and swift heavy ions exhibit same diffraction diagrams [16]. From these results, some authors claim the apparition of a new phase under irradiation for this spinel [7,8]. They suppose that the new phase can be described by the $Fm\bar{3}m$ space group. Following these authors [8], a simulation of the X-ray diffraction diagrams with Mg and Al cations in 4a positions and anions in 4b positions of the $Fm\bar{3}m$ space group leads to a non-null peak near 38° (corresponding to the (2 2 2) reflection of the $Fd\bar{3}m$ group) which does not appear in the experimental X-ray diffraction diagram (Fig. 6). This space group with such Wickoff positions for atoms cannot correctly explain the X-ray diffraction patterns observed on the irradiated $MgAl_2O_4$ spinel.

The atomic structure factors of Mg and Al atoms are quite similar, and it is not easy to distinguish between these two species by analysing only MET and X-ray diffraction diagrams. Based on the analysis of neutron diffraction diagrams on $MgAl_2O_4$ single crystal irradiated by neutrons at high fluences [9] and by analogy to the results presented above on $ZnAl_2O_4$, we suppose that the irradiation by swift heavy ions leads to a random distribution of Mg and Al cations in this spinel. The best way to fit experimental Rietveld diagrams is to use the $Fd\bar{3}m$ space group and to modify the occupation sites of Al and Mg atoms in 8a and 16d Wickoff positions. Because experimental diagrams possess few peaks and many parameters are needed to describe Bragg peaks (Table 1), Rietveld refinements cannot converge using such a space group.

To take this point into account in the description of this irradiated spinel, a fictitious atom, called SP, has been created. The atomic structure factor of this fictitious SP atom, describing a random occupation of cations sites in this spinel, is an average between Mg (0.33 atomic fraction) and Al (0.66 atomic fraction) atomic structure factors. Fig. 7 presents the atomic structure factors of Mg, Al and of the fictitious SP atom. The random distribution of Al and Mg cations on Wickoff sites of this spinel, induced by irradiation, is then equivalent to the apparition of the SP atoms in 8a and 16d sites in the $Fd\bar{3}m$ space group. This distribution modifies the crystallographic space group from $Fd\bar{3}m$ to $Fm\bar{3}m$ (Figs. 8 and 9), and leads to a reduction by two of the unit cell parameter. In our Rietveld refinements, experimental X-ray diffraction diagrams were then fitted in the $Fm\bar{3}m$ space group with SP atoms in 4a and 8c Wickoff positions (the 8c sites were empty in [8]). No peak appears near 38° on the simulated X-ray diagram, in agreement with experiments (Fig. 6). The important value of the GofF is due to the very low value of R_{exp} (data over collected) as it is the case for $ZnAl_2O_4$. R_{Bragg}

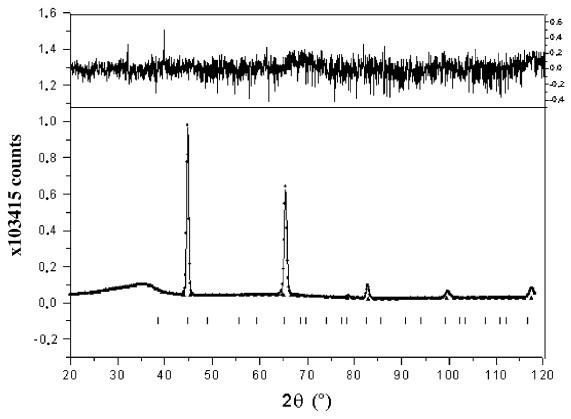

Fig. 6. Rietveld refinement on an irradiated $MgAl_2O_4$ sample.

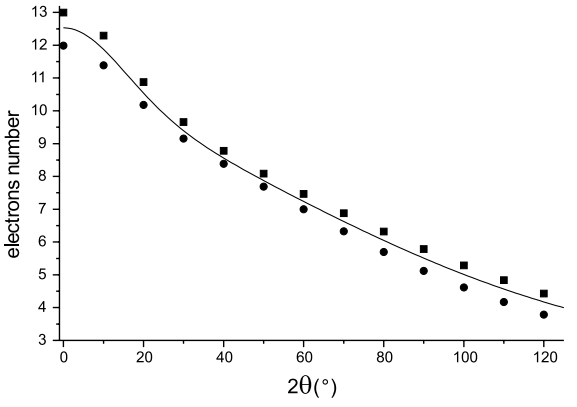

Fig. 7. Atomic form factor associated to a fictitious atom composed of Al and Mg atoms. The form of this atomic form factor lies between Al form factor (●) and Mg form factor (■). This atomic form factor $(0.66f_{Al} + 0.33f_{Mg})$ was fitted by the classical equation $f = a_0 + \sum_{i=1}^{4} a_i \exp(-b_i \times (\frac{\sin(\theta)}{\lambda})^2)$. The quality of the fit is given by $\chi^2 = 3 \times 10^{-4}$ and $1 - \rho^2 = 10^{-6}$.

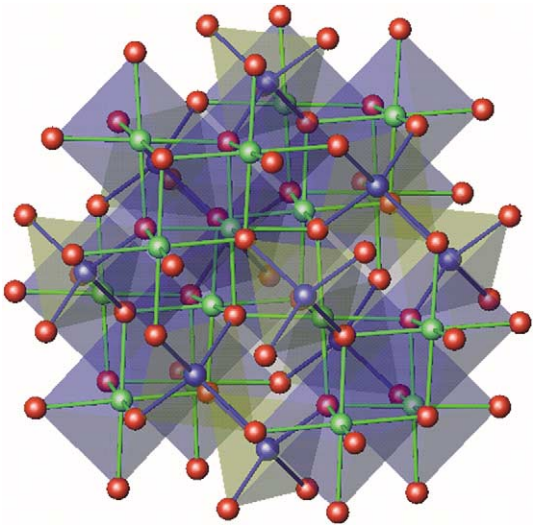

Fig. 8. Cell of the unirradiated $MgAl_2O_4$ spinel. Al (green) Mg (blue) and O (red) atoms are plotted. The different tetrahedra (yellow) and octahedra (blue) are drawn. The unit cell parameters and atomic positions used are results from the above Rietveld refinement. In this figure, all sites are occupied.

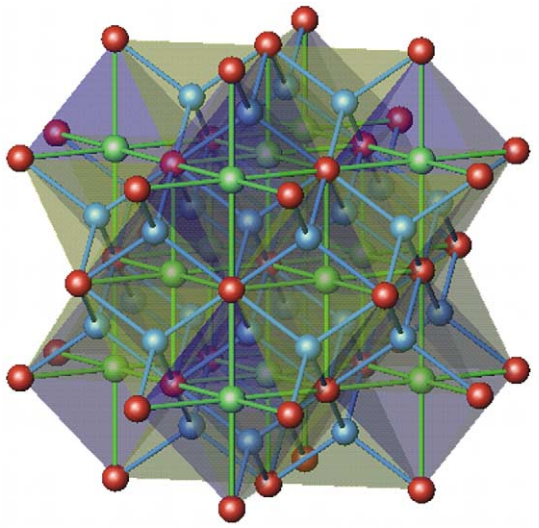

Fig. 9. Cell of the irradiated $MgAl_2O_4$ spinel. The SP atom at the centre of each octrahedron is drawn in green and SP atoms at the centre of tetrahedron are drawn in blue. The unit cell parameters and atomic position used are results from the above Rietveld refinement. In this figure, all sites are occupied.

is quite correct. Fig. 9 presents atomic polyhedra in the irradiated $MgAl_2O_4$ spinel obtained by Rietveld refinement.

From this analysis, it seems that the irradiation of spinels by neutrons or ions (swift heavy ions and low energetic ions at cryogenic temperature) leads only to an order–disorder phase transition mixing of the A and B cations in AB_2X_4 spinels. In the case of $MgAl_2O_4$, an extinction appears as in KCl due to similarities between atomic for factors of these ions, leading to a division by two of the unit cell. Therefore, such a description is purely due to the technique used to investigate the evolution of the material and does not have any physical signification: the same effect is observed with X-ray and TEM diffraction over a large range of the inversion parameter around 2/3 and not with neutron diffraction [2]. In fact, neutron form factors for Mg and Al are quite different and such an accidental extinction does not appear in these diffraction diagrams.

Moreover, the bond lengths calculated from Rietveld refinement for tetrahedra and octahedra on the irradiated $MgAl_2O_4$ spinel are equal to 0.1745 and 0.2015 nm respectively, whereas their values are 0.1908 and 0.1928 nm for the unirradiated samples. These results are consistent with results obtained on $ZnAl_2O_4$: in the latter, increasing the inversion parameter leads to the increasing of the octahedral bond length (from 0.1919 to 0.1942 nm) and a decreasing of the tetrahedral bond length (from 0.1938 to 0.1901 nm).

Irradiated at similar stopping powers (14 keV nm^{-1} for $MgAl_2O_4$ and 9 keV nm^{-1} for $ZnAl_2O_4$), Rietveld refinements clearly show that the inversion of Mg cations is more important than that of Zn. This fact can be easily explained comparing the empirical site preference energies of both spinels [17].

For $MgAl_2O_4$, a clear shift of the unit cell parameter is observed on the irradiated sample. This shift cannot be explained by the important increasing of the Mg cation disordering. Moreover, the Hall Williamson plot of the peaks broadening (Table 2) exhibits a local strain field in the irradiated sample. All these facts can be understood. The amorphous tracks produced during irradiation (cf. Fig. 6) compress the crystalline area inducing macroscopic and microscopic strain fields in the samples.

3.2. Raman spectroscopy

Using the group theory [18], it is possible to define the number of peaks expected on Raman spectra both for the unirradiated and the irradiated samples. For the $Fd\bar{3}m$ space group, the reducible representation at zone centre of the unirradiated sample is (using the rhomboedral unit cell):

$$\Gamma = 3F_{2g} \oplus A_{1g} \oplus E_g \oplus F_{1g} \oplus 4F_{1u} \oplus 2F_{2u} \oplus 2E_u \oplus 2A_{2u}.$$

Table 3 shows the evolution of Raman peaks on unirradiated and irradiated samples. The Raman spectra of the unirradiated samples are similar to that already observed on synthetic Raman spectra [19,20]. In agreement with Rietveld refinements, a peak located at

Table 3
Comparison of Raman peaks measured on unirradiated and irradiated $MgAl_2O_4$ samples

IR	F_{2g}	E_g	F_{2g}	F_{2g}		A_{1g}
Peaks positions (cm^{-1}) [19]	311	410	492	671		772
Unirradiated sample						
Peaks positions (cm^{-1})	306.9(1)	406.0(1)	–	670.0(2)	723.0(7)	766.0(2)
peaks width (cm^{-1})	17(1)	27(1)	–	21.7(5)	12.5(2)	15.7(4)
integrated intensities (cps)	2.8(1)	37.0(2)	–	6.3(2)	1.2(1)	9.0(1)
Irradiated sample						
peaks positions (cm^{-1})	306(1)	407.0(2)	477(1)	672.3(7)	721(2)	767.3(4)
peaks width (cm^{-1})	4.8(2)	41.39	85(7)	21.9(3)	50.6(6)	15.0(1)
integrated intensities (cps)	0.4(1)	43.9(8)	30.8(2)	5.6(8)	10.0(1)	5.0(3)

The Raman peaks of both Raman spectra were fitted by Lorentzian curves. The values of χ^2 were equal to 4×10^{-4} and 12×10^{-4} for unirradiated and irradiated samples.

727 cm^{-1}, associated to the stretching of Al–O tetrahedra [20], is observed on the Raman spectra.

For the crystallographic structure proposed by some authors [8], similar calculations give

$$\Gamma = 2F_{1u}.$$

No Raman peaks should appear if the structure proposed was correct. This is clearly not the case (Fig. 10).

Raman spectra were collected on unirradiated and irradiated $MgAl_2O_4$ samples. On the irradiated sample, an unusual background is observed both on the Stockes and anti-Stockes spectra. The amorphisation of the spinel and/or the existence of colour centres induced by irradiation seem to be responsible of this background. These defects fill the band gap and the laser light excites not only vibrational states but also some electronic vibrations associated to these defects.

Fig. 10 presents a comparison of Raman spectra between the unirradiated (a) and irradiated (corrected of the background) (b) MAl_2O_4 samples. On the initial spectra (a), measured Raman peaks agree with previous analyses [19,20]. The peak at 723 cm^{-1} is assigned to an Al–O stretching vibration of AlO_4 tetrahedra [20]. This implies that some Al ions are in tetrahedral sites in agreement with Rietveld refinements on the unirradiated samples (Table 2). On the irradiated samples (b), a large broadening of the intense 407 and 721 cm^{-1} peaks occurs. This broadening is associated to the bending (407 cm^{-1}) and the stretching of AlO_4 tetrahedra in agreement with an increase of the inversion parameter in the spinel during the irradiation. The extra peak at 477 cm^{-1} cannot be assigned to Raman or infrared frequencies of the unirradiated spinel due to defects [19]. Based on the measures of phonon density of states (PDOS) in MgO [21], this extra peak may be linked to the PDOS of amorphous $MgAl_2O_4$ detected in the irradiated spinel by X-ray diffraction (Fig. 6).

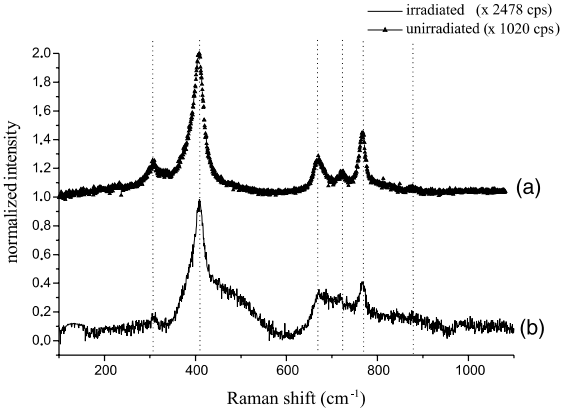

Fig. 10. Comparison of the Raman spectra collected on unirradiated (curve a) and irradiated (curve b) $MgAl_2O_4$ spinels.

In order to confirm this point, we try to calculate Raman, infrared frequencies and PDOS in the rigid ion model, but numerous interatomic potentials proposed [22,23] were not able to correctly phonon dispersion curves and the PDOS in the $MgAl_2O_4$ spinel.

4. Discussion

From these results the following points clearly appear:

(1) First, irradiation by swift heavy ions on $MgAl_2O_4$ leads to X-ray diffraction diagrams comparable to MET diffraction diagrams obtained by irradiation of low energetic ions at cryogenic temperatures.

(2) Secondly, experiments done with swift ions on $ZnAl_2O_4$ show that an order–disorder transition occurs during irradiation.

(3) Moreover, we have shown that an order–disorder transition without any modification of the space group occurs in $MgAl_2O_4$ as in $ZnAl_2O_4$ during irradiation.

Following O'Neill and Dollase [2], it is possible in the mean field theory to describe the evolution of spinels as a function of temperature. This evolution shows a modification of the inversion parameter, i.e. the mixing of cations on sites 8a and 16d of the $Fd\bar{3}m$ space group. To describe this evolution, it is possible to compute a free energy as a function of an order parameter η, a linear function of the inversion parameter.

Taking into account only the configurational entropy due to substitution of cations, and describing the internal energy in term of long range electrostatic potential (Madelung constant) and short range pair potentials (Born Mayer potentials), the Gibbs energy of the spinel can be described as a function of the order parameter. Carpenter and Salje [24–26] expressed the Gibbs energy as a polynomial of the order parameter in the Landau framework. This Gibbs potential can be written as

$$G \propto -h\eta + \frac{a}{2}(T - T_C)\eta^2 + \frac{1}{6}c\eta^6,$$

where h, a, T_C and c are phenomenological coefficients. Numerical values for these coefficients exist for $MgAl_2O_4$ [15] or can be obtained from data for $ZnAl_2O_4$ [2].

The first term in G strictly forbidden in the Landau phase transition is used to describe the extra energy cost associated to the AlO_4 formation. This term is responsible for the removal of the critical temperature leading to the so-called non-convergent order–disorder transition in spinels.

As mentioned above, analysing formally the behaviour of spinels under irradiation, i.e. the order–disorder transition, is analogous to analyse the behaviour of the displacive phase transition induced by irradiation of ZrO_2 by swift and low ions [27]. The analysis of the ZrO_2 phase transition is roughly understood. The ejection of electrons in the swift ion path or during displacement cascades leads to a modification of the ionic dielectric constant of the material, i.e. a coupling between expulsed delta electrons and ions forming the skeleton of the target. This induces fluctuations of the ionic polarisation and a displacement of the order parameter (in the case of ZrO_2, this order parameter is related to a shift of the oxygen atoms in the cell). A similar mechanism can explain the order–disorder transition in spinels, replacing the oxygen shift by the inversion parameter in the Landau Ginzburg kinetic equation [27].

5. Conclusion

The aim of this work was to study the behaviour of some spinels under irradiation using X-ray diffraction. Moreover, Raman spectroscopy is used to confirm results obtained by the Rietveld refinement made on X-ray diffraction diagrams. To carry on this analysis, $MgAl_2O_4$ and $ZnAl_2O_4$ samples were irradiated by high energetic ions. The bombardment of $MgAl_2O_4$ and $ZnAl_2O_4$ spinels by swift ions allows to probe an important volume by X-rays and then to obtain accurate information especially on the space group of the irradiated samples. The analysis of Rietveld refinement on these two spinels clearly shows an order–disorder transition under irradiation without any modification of their space group. Such a transition has already been observed at equilibrium at high temperature. Nevertheless, the order parameter (i.e the inversion parameter) reaches more important values under irradiation. These insulating materials, with a band gap of about 9 and 4 eV exhibit a behaviour similar to ZrO_2, an other insulator with a band gap of about 6 eV: they present either an order–disorder transition or a displacive transition which can be described in the Landau theory framework, the transition being initiated either by irradiation by low energetic or swift ions or observed at equilibrium at high temperature. Works are in progress in our laboratory to develop a possible model including irradiation effects in this class of materials.

Acknowledgements

We acknowledge Dr N. Pellerin (CRMHT-CNRS. Orleans) for RMN measures on $MgAl_2O_4$ and $ZnAl_2O_4$ spinels.

References

[1] G. Summers, G. White, K. Lee, J. Crawford, Phys. Rev. B 21 (6) (1980) 2578.
[2] H. O'Neill, W. Dollase, Phys. Chem. Miner. 20 (1994) 541.
[3] I. Afanasyev-Charkin, R. Dickerson, D. Cook, B. Benett, V. Gritsyna, K. Sickafus, J. Nucl. Mater. 289 (2001) 110.
[4] S. Zinkle, H.J. Matzke, W. Skuratov, Mater. Res. Soc. Symp. Proc. 540 (1999) 289.
[5] C. Kinoshita, K. Fukumoto, K. Fukuda, F. Garner, G. Hollenberg, J. Nucl. Mater. 219 (1995) 143.
[6] N. Yu, K. Sickafus, M. Nastasi, Philos. Mag. Lett. 70 (1994) 235.
[7] R. Devanathan, K. Sickafus, N. Yu, M. Natasi, Philos. Mag. Lett. 72 (3) (1995) 155.
[8] M. Ishimaru, I. Afanayev-Charkin, K. Sickafus, Appl. Phys. Lett. 76 (18) (2000) 2556.
[9] K. Sickafus, A. Larson, N. Yu, G. Hollenberg, F. Garner, R. Bradt, J. Nucl. Mater. 219 (1995) 128.
[10] C. Kinoshita, J. Nucl. Mater. 191 (1992) 67.
[11] A. Seeram, L. Hobbs, Mater. Res. Soc. Symp. Proc. 373 (1995) 359.
[12] D. Simeone, D. Gosset, J.L. Béchade, CEA-R 5975 report, 2001.
[13] A. Klug, X-ray Diffraction Procedures, Wiley, New York, 1966.
[14] J.F. Berar, G. Baldinozzi, CPD Newsletter 20 (1998) 3.

[15] S. Redfern, R. Harrison, H. O'Neill, D. Wood, Am. Mineral. 84 (1999) 299.
[16] S. Zinkle, V. Skuratov, Nucl. Instrum. and Methods 141 (1998) 737.
[17] A. Navrotsky, O. kleppa, J. Inorg. Nucl. Chem. 29 (1961) 2701.
[18] D. Rousseau, R. Bauman, S. Porto, J. Raman Spectrosc. 10 (1981) 253.
[19] M. O'Horo, A. Frisillo, W. White, J. Phys. Chem. Solids 34 (1973) 28.
[20] H. Cynn, Phys. Rev. B 45 (1) (1992) 500.
[21] H. Bliz, W. Kress, Phonon dispersion relations in insulators, in: Solid State Science, vol. 10, Springer, Berlin, 1979.
[22] S. Mo, W. Ching, Phys. Rev. B 54 (23) (1996) 16555.
[23] R. Mittal, S. Chaplot, N. Choudhury, Phys Rev B 64, 94302.
[24] M. Carpenter, E. Salje, Am. Mineral. 79 (1994) 1068.
[25] M. Carpenter, R. Powell, E. Salje, Am. Mineral. 79 (1994) 1053.
[26] E. Salje, Phys. Chem. Miner. 15 (1988) 336.
[27] D. Simeone, D. Gosset, J.L. Bechade, A. Chevarier, J. Nucl. Mater. 300 (2002) 27.